Adsorption of chlorine on Ag(111): No subsurface Cl at low coverage

Paola Gava,[1] Anton Kokalj,[2,1] Stefano de Gironcoli,[1] and Stefano Baroni[1]
[1]*Scuola Internazionale Superiore di Studi Avanzati (SISSA), I-34014 Trieste, Italy and INFM DEMOCRITOS National Simulation Center, I-34014 Trieste, Italy*
[2]*Jožef Stefan Institute, SI-1000 Ljubljana, Slovenia*
(Received 8 May 2008; revised manuscript received 17 September 2008; published 23 October 2008)

The adsorption of molecular and atomic chlorine on perfect Ag(111) surface has been studied and characterized by means of extensive density-functional-theory calculations. For the molecular adsorption, we find that the dissociation of Cl_2 proceeds with an almost vanishing barrier. As for the adsorption of atomic Cl, on-surface, subsurface, and substitutional adsorptions are considered as a function of the coverage. At coverage lower than 1/2 ML, the on-surface adsorption displays the most exothermic chemisorption energies, whereas the mixed on-surface+subsurface and on-surface+substitutional adsorption modes become competitive with pure on-surface adsorption at about 1/2 ML of coverage and at higher coverages even preferred. The analysis of the adsorption free energy as a function of chlorine chemical potential reveals that the on-surface $(\sqrt{3} \times \sqrt{3})R30°$ adsorption phase is thermodynamically the most stable over a very broad range of Cl chemical potential. The mixed adsorption modes become thermodynamically more stable at high coverage for values of the Cl chemical potential that are substantially larger than those needed to form silver chloride. This finding seems to indicate that the formation of mixed adsorption phases, if they would ever occur, cannot be due to thermodynamic equilibrium but can only result from kinetic effects. We also find that the presence of open surface steps does not stabilize the subsurface Cl adsorption at low coverage. However due to the stronger Cl-surface interaction near steps, the mixed on-surface+subsurface adsorption on Ag(210) at high coverage becomes thermodynamically the most stable phase at Cl chemical potential close to that needed for the formation of bulk AgCl.

DOI: 10.1103/PhysRevB.78.165419 PACS number(s): 68.43.Bc, 68.43.Fg, 68.35.Md, 68.47.De

I. INTRODUCTION

Silver surfaces have been studied extensively mainly because silver displays remarkably good catalytic properties in ethylene epoxidation reaction, which is one of the most important selective oxidation processes occurring on metal catalysts.[1] In presence of promoters, such as Cl and Cs, the selectivity of this reaction toward ethylene epoxide (EO), at high temperature and high pressure, is up to 80%.[1–3]

Recently, Linic and Barteau[4] suggested, on the basis of density-functional-theory (DFT) calculations, that Cs on-surface adatoms promote the formation of EO against the acetaldehyde (Ac) due to dipole-dipole lateral interaction between the transition state (TS) and Cs adatom, which is more favorable for the TS leading to EO than for the TS leading to Ac. As for the electronegative Cl promoter, it is commonly believed that it is adsorbed subsurface[5–7] and by analogy with the Cs case Linic and Barteau[4] argued that Cl would have a similar effect as Cs, *provided* it is adsorbed subsurface.

The interaction of chlorine with Ag surfaces has been extensively studied by experiments[5,6,8–13] and computer simulations.[14–17] The computational studies,[14–17] however, deal mainly with on-surface chlorine adsorption. For this reason we address in this paper the feasibility of Cl subsurface adsorption with emphasis to shed some light on the mechanisms for Cl incorporation below the surface. In particular we address the on-surface, subsurface, and substitutional adsorptions of atomic Cl on Ag(111)—which is the majority surface exposed on metal particles. We also present results for the adsorption of Cl_2 molecule on Ag(111).

As for the subsurface adsorption of atomic oxygen, it has been demonstrated[18–23] that it goes subsurface only after some critical on-surface coverage, which in the case of silver is around 1/2 ML. It is reasonable, therefore, to expect that also Cl will penetrate into subsurface only after some critical on-surface coverage. A pivotal question we address in this work is to determine the critical coverage at which Cl atoms start to adsorb below the surface. Since low coordinated defects, such as step edges, have been shown to assist the penetration of atomic oxygen into subsurface,[24,25] we also discuss how the presence of low coordinated defects could affect the adsorption of Cl into subsurface. For this purpose, we deliberately chose a very open surface, such as Ag(210), which consists of one-atom row wide (110) and (100) nanofacets.

II. COMPUTATIONAL DETAILS AND DEFINITIONS

All presented results are obtained by *ab initio* calculations, in the framework of DFT, using the Perdew-Burke-Ernzerhof (PBE) (Ref. 26) generalized gradient approximation (GGA) for the exchange-correlation functional. Core electrons are taken into account using the pseudopotential method, with ultrasoft pseudopotentials.[27] Plane-wave basis set is used to describe valence electron wave functions and density up to kinetic-energy cutoffs of 27 and 216 Ry, respectively. The Brillouin-zone (BZ) integration has been performed using the Gaussian-smearing special-point technique,[28,29] with a smearing parameter of 0.03 Ry. Calculations have been performed using the PWSCF code[30] of the QUANTUM ESPRESSO distribution.[31] Molecular graphics were

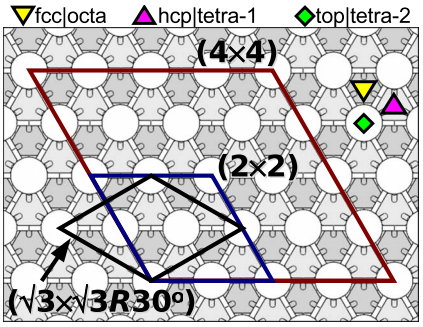

FIG. 1. (Color online) Representation of different supercells and sites used in this work to model adsorption of chlorine on Ag(111): (4×4), (2×2), and $(\sqrt{3}\times\sqrt{3})R30°$ supercells are drawn with red, blue, and black lines, respectively. The yellow down-triangle represents the on-surface fcc site and the subsurface octahedral (octa) site, beneath fcc (labeled as fcc|octa). The two different tetrahedral sites are labeled as tetra-1 and tetra-2. Tetra-1 is located beneath the hcp site (magenta up-triangle, hcp|tetra-1) and tetra-2 is located beneath a surface Ag atom (green diamond, top|tetra-2). Bridge site is not shown and is located between two nearest Ag surface atoms.

produced by the XCRYSDEN graphical package.[32]

Ag surfaces have been modeled by periodically repeated slabs, consisting of four layers for the (111) surface and seven layers for the (210) surface. The bottom layer for the (111) surface and the two bottom layers for the (210) surface are kept fixed to the bulk positions, while all other degrees of freedom are relaxed. Cl atoms are adsorbed on one side. Dipole correction, to cancel out the fictitious dipole created perpendicular to the surface, is applied to the case of 1/4 ML of Cl on Ag(111), adsorbed on fcc site. The energy difference between calculations with and without dipole correction is small, 0.01 eV. For this reason we performed all other calculations without dipole correction. All structures are relaxed until forces on atoms are less than 0.02 eV/Å. The thickness of vacuum region is set to 15 Å. The in-plane lattice spacing in surface calculations was determined from the calculated equilibrium bulk lattice parameter of 4.16 Å. For comparison purposes, we also performed a few calculations of O adsorption on Ag(111) using analogous computational parameters.

A. Supercells and sites

Different Cl coverages on Ag(111) were modeled using different supercells. In particular, for 1/16 and 1/9 ML we used (4×4) (Fig. 1, red line) and (3×3) supercells, respectively, whereas 1/4, 1/2, and 3/4 ML were modeled by (2×2) supercells (Fig. 1, blue line). For 1/3 and 2/3 ML we used $(\sqrt{3}\times\sqrt{3})R30°$ supercell (Fig. 1, black line). BZ integrations were performed using $(2\times2\times1)$, $(3\times3\times1)$, $(4\times4\times1)$, and $(4\times4\times1)$ uniformly shifted k-point mesh for the (4×4), (3×3), (2×2), and $(\sqrt{3}\times\sqrt{3})R30°$ supercells, respectively. All calculations on Ag(210) were done using
(2×1) supercell and $(4\times7\times1)$ shifted k-point mesh.

On-surface and subsurface adsorption sites on Ag(111) are also shown in Fig. 1, where the lateral position of the sites above and below the surface is labeled as on surface|subsurface. There are four different on-surface adsorption sites: fcc, hcp, bridge (not shown), and top. As for the adsorption below the top Ag layer, we considered Cl atoms adsorbed into octahedral (labeled as octa) and two tetrahedral interstitials, labeled as tetra-1 and tetra-2. The octa site is located below an fcc site between the surface and the first subsurface layer. Analogously, the tetra-1 site is located below an hcp site, whereas the tetra-2 site is located beneath a surface Ag atom and above three Ag atoms of the first subsurface layer.

B. Energy equations

The binding energy of Cl_2 gas-phase molecule is calculated as $E_b=(E_{Cl_2}-2E_{Cl})$, where E_{Cl_2} is the total energy of the molecule in the gas phase and E_{Cl} is the total energy of spin-polarized atomic Cl. The adsorption energy for molecular Cl_2 on Ag surface is

$$E_{ads}^{Cl_2}=E_{Cl_2/Ag}-(E_{Ag}+E_{Cl_2}), \tag{1}$$

where $E_{Cl_2/Ag}$ is the total energy of adsorption system and E_{Ag} is the total energy of a clean Ag surface. The average chemisorption energy for dissociative adsorption of chlorine is calculated as

$$E_{chem}=\frac{1}{n}\left[E_{Cl/Ag}-\left(E_{Ag}+\frac{n}{2}E_{Cl_2}\right)\right], \tag{2}$$

where n is total number of Cl atoms adsorbed on Ag surface and $E_{Cl/Ag}$ is the total energy of adsorption system.

The substitutional chemisorption energy, per Cl atom, of n Cl atoms into n vacancy on Ag(111) is given by

$$E_{chem}^{subst}=\frac{1}{n}\left[E_{Cl/vac}+nE_{bulk}-E_{slab}-\frac{n}{2}E_{Cl_2}\right], \tag{3}$$

where $E_{Cl/vac}$ is the total energy of the substitutional adsorption system, E_{bulk} is the energy of a Ag atom in the bulk, and E_{slab} is the total energy of the slab without the vacancy. This definition of chemisorption energy includes the vacancy formation energy, which is given by

$$E_f=\frac{1}{n}[E_{vac}+nE_{bulk}-E_{slab}], \tag{4}$$

where E_{vac} is the total energy of the Ag slab with n vacancies. In the case of mixed substitutional+on-surface adsorption, the net chemisorption energy is calculated as

$$E_{chem}^{subst}=\frac{1}{m}\left[E_{Cl/vac}+nE_{bulk}-E_{slab}-\frac{m}{2}E_{Cl_2}\right], \tag{5}$$

where m is the total number of Cl atoms, n the number of vacancies and substitutionally adsorbed Cl atoms, and $m\geq n$.

We also define the gross chemisorption energy of n Cl atoms into n preformed vacancies as

TABLE I. Calculated adsorption energies and structural parameters for Cl_2 adsorption on Ag(111), with its axis perpendicular to the surface. Labels d_{Cl-Cl} and d_{Cl-Ag} designate Cl–Cl and Cl–Ag bond lengths, respectively. For comparison, the calculated bond distance of gas-phase Cl_2 molecule is also reported.

Site	$E_{ads}^{Cl_2}$ (eV)	d_{Cl-Ag} (Å)	d_{Cl-Cl} (Å)
fcc	−0.61	2.70	2.34
hcp	−0.60	2.70	2.34
Bridge	−0.56	2.64	2.31
Top	−0.35	2.59	2.18
Gas phase			2.00

$$E_{chem}^{vac} = \frac{1}{n}\left[E_{Cl/vac} - E_{vac} - \frac{n}{2}E_{Cl_2}\right]. \quad (6)$$

On the basis of our computational parameters, e.g., convergence with respect to plane-wave cutoff and k-point density, we estimate an error in the adsorption energies of 0.03 eV.

C. Structural parameters

To facilitate the characterization of Cl/Ag structures, we define a few structural parameters. The interlayer distance between the surface and subsurface Ag layers, d_{12}, is calculated as the difference between the average height of surface Ag atoms and the average height of subsurface Ag atoms. The relaxation of the surface layer, Δd_{12}, is the difference between the d_{12} and the ideal bulk interlayer spacing.

Upon Cl adsorption, the vertical buckling (or corrugation) of surface Ag atoms can be substantial. As an approximate measure of the corrugation, we define the parameter h_{Ag}^{surf} as the difference in height between the highest and lowest Ag atoms in the surface layer.

$d_{Cl\text{-}Ag}^{on}$ ($d_{Cl\text{-}Ag}^{sub}$, $d_{Cl\text{-}Ag}^{subst}$) is the average distance between on-surface (subsurface, substitutional) Cl atoms and nearest-neighbor Ag atoms. $\Delta z_{Cl\text{-}Ag}^{on}$ ($\Delta z_{Cl\text{-}Ag}^{sub}$, $\Delta z_{Cl\text{-}Ag}^{subst}$) is the distance between the average height of the on-surface (subsurface, substitutional) Cl atoms and the average height of surface Ag atoms. Other more obvious parameters will be explained when used.

III. RESULTS

A. Cl_2 on Ag(111)

In this section we present results for isolated Cl_2 molecule and its molecular adsorption onto Ag(111) surface. Isolated Cl_2 molecule displays a bond length of 2.00 Å and a binding energy of −2.76 eV. These results are in reasonable agreement with experiments,[14] where the measured bond length is 1.99 Å and the binding energy is −2.48 eV, and with previous GGA results,[14] where bond length is 2.05 Å and the binding energy is −2.69 eV.

In Table I we report several adsorption configurations of Cl_2 molecule on Ag(111) with its axis perpendicular to the surface. The fcc and hcp sites result to be the most stable, with an adsorption energies of −0.61 and −0.60 eV, respectively. The adsorption on bridge site is only slightly less stable, with an adsorption energy of −0.56 eV, whereas the top site is the least stable with an adsorption energy of −0.35 eV.

The molecular bond length is elongated substantially upon adsorption by 0.34 Å in the most stable hollow sites and by 0.18 Å in the least stable top site (see Table I). The Cl-Ag bond distances are between 2.7 and 2.6 Å, depending on the adsorption site. Similar results for such Cl_2 adsorption geometry on fcc were found by de Leeuw *et al.*[16] These authors predicted a smaller adsorption energy, −0.44 eV, a Cl-Cl bond length of 2.40 Å, and a distance between the closest Cl atom and Ag surface of 2.65 Å.

We also investigated molecular adsorption of Cl_2 with its axis tilted with respect to the surface normal. According to our calculations, the potential-energy surface (PES) results to be extremely flat. For this reason, we performed a careful climbing image nudged elastic band (CI-NEB) (Refs. 33 and 34) calculation for the dissociation of the Cl_2 molecule, starting from the molecule adsorbed perpendicularly into the fcc site. The result is displayed in Fig. 2, and it shows the flatness of PES around the initial state. The dissociation proceeds with an almost vanishing barrier of 0.03 eV. This is in agreement with the experimental observation that Cl_2 adsorbs dissociatively on Ag.[8] The dissociation is highly exothermic, by ≈1.5 eV/molecule (see Fig. 2), but the precise value depends on the chlorine coverage.

Extremely small dissociation barrier is not surprising because of the substantially elongated Cl–Cl bond in the molecularly adsorbed form (Table I). Indeed, this bond is almost

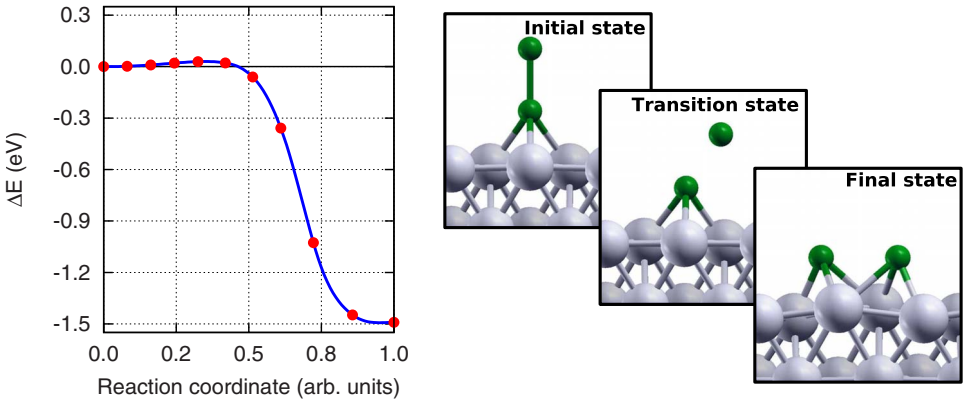

FIG. 2. (Color online) Reaction energy profile for dissociation of Cl_2 molecule. The corresponding initial, transition, and final states are also shown. The potential-energy surface around the initial state is very flat, and dissociation proceeds with vanishing barrier within the estimated accuracy of our calculation.

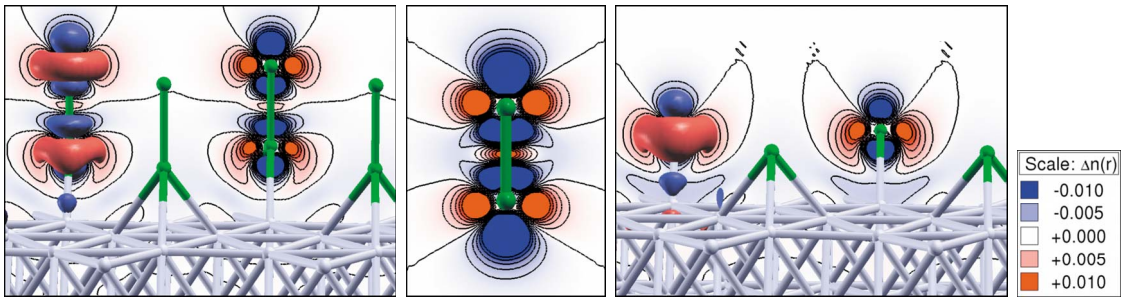

FIG. 3. (Color online) (a) Charge density difference, $\Delta n(\mathbf{r})$, for Cl_2 adsorbed perpendicular to the surface on fcc site, calculated as $\Delta n(\mathbf{r})=n_{Cl_2/Ag}(\mathbf{r})-[n_{Cl'}(\mathbf{r})+n_{Cl''}(\mathbf{r})+n_{Ag}(\mathbf{r})]$, where labels Cl′ and Cl″ stand for the two individual Cl atoms of the Cl_2 molecule. (b) $\Delta n(\mathbf{r})$ of isolated Cl_2 molecule, $\Delta n(\mathbf{r})=n_{Cl_2}(\mathbf{r})-[n_{Cl'}(\mathbf{r})+n_{Cl''}]$. (c) $\Delta n(\mathbf{r})$ of Cl atom chemisorbed into the fcc site, $\Delta n(\mathbf{r})=n_{Cl/Ag}(\mathbf{r})-[n_{Cl}(\mathbf{r})+n_{Ag}(\mathbf{r})]$. Contours are drawn in linear scale from $-0.01e/a_0^3$ to $0.01e/a_0^3$, with the increment of $0.002e/a_0^3$. Isosurfaces of $\pm 0.005e/a_0^3$ are also shown. The blue color represents the electron deficit regions, while the electron excess regions are colored in red (i.e., charge flows from blue to red regions).

broken in the adsorbed Cl_2 as can be seen from Fig. 3(a), where charge-density differences, $\Delta n(r)$, between the adsorption system and its constituents are presented, $\Delta n(\mathbf{r})=n_{Cl_2/Ag}(\mathbf{r})-[n_{Cl'}(\mathbf{r})+n_{Cl''}(\mathbf{r})+n_{Ag}(\mathbf{r})]$ (the labels Cl′ and Cl″ stand for the two individual Cl atoms of the Cl_2 molecule). Indeed, there is almost no accumulation of charge between the two Cl atoms if compared with Fig. 3(b), where the $\Delta n(r)$ of isolated Cl_2 is shown. Moreover the charge redistribution in Fig. 3(a) around the bottom Cl atom (the one bonded to the surface) is similar to that of chemisorbed Cl atom, shown in Fig. 3(c).

The extent of the Cl–Cl bond break in the adsorbed molecule can be further characterized by means of the atomic projected densities of states (PDOSs). In Fig. 4 we display and compare the PDOSs projected onto individual Cl atoms and onto the Ag atom to which the molecule binds for three different systems (from top to bottom): (1) Cl_2 molecule high above the surface (6 Å), (2) the equilibrium Cl_2 adsorbed perpendicularly into the fcc site, and (3) the Cl atom chemisorbed into the fcc site. When the molecule is high above the surface (Fig. 4, top panel), the molecular levels are clearly identified as peaks in the PDOS. Top panel of Fig. 4 displays three molecular peaks below the Fermi level, which are σ_g, π_g, and π_u. The former lies about 1.5 eV below the metal d band and is the bonding combination of the two p_z orbitals (z is along molecular axis), whereas the latter two—which lie at the bottom and top of the d band—are doubly degenerated π orbitals: π_g (π_u) is the bonding (antibonding) combination of the two p_x and/or the two p_y orbitals. The σ_u lowest unoccupied molecular-orbital (LUMO) state is located just above the Fermi level: this is the antibonding combination of the two p_z orbitals. The two lowest lying valence states of Cl_2 (σ_g and σ_u, bonding and antibonding combinations of the $3s$ orbitals of the two Cl atoms) are located about −19 and −15 eV below the Fermi level (not shown).

Upon adsorption of Cl_2 (Fig. 4, middle panel) the molecular electronic structure changes completely, and individual PDOSs of the two Cl atoms are rather different. The top Cl atom displays an atomiclike narrow peak at −1 eV below the Fermi level. This peak consists of the atomic p levels and comprises about four electrons as indicated by the integrated PDOS shown by the thin blue line. On the other hand, the hybridization between the bottom Cl atom (i.e., the one bonded to the surface) and the surface d states is quite substantial and is similar to that for the chemisorbed Cl at fcc site (Fig. 4, bottom panel).

The integrated PDOS up to the Fermi level corresponds to Löwdin charges. For the Cl_2 molecule adsorbed into the fcc

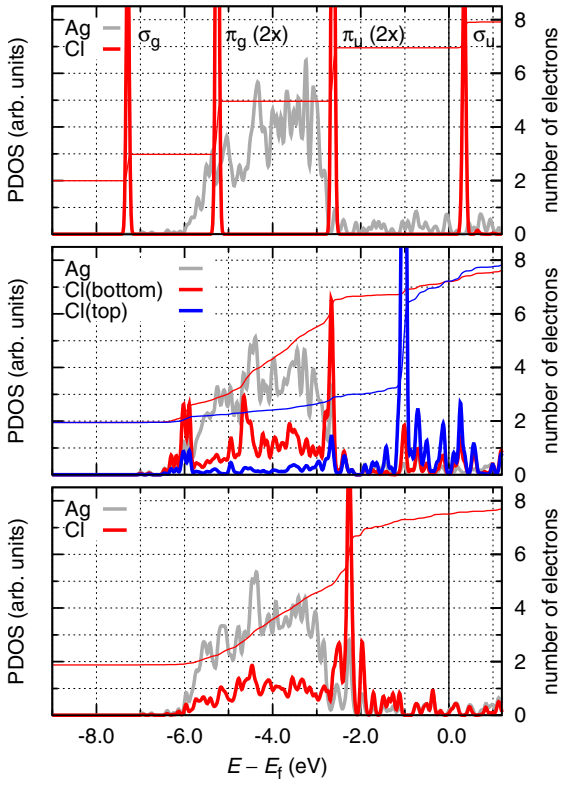

FIG. 4. (Color online) Density of electronic states projected (PDOS, left axis) onto individual Cl atoms (red and blue curves) and onto Ag surface atom underneath (gray curve). From top to bottom: (1) Cl_2 molecule high above the surface (6 Å), (2) equilibrium Cl_2 adsorbed perpendicularly onto the fcc site, and (3) Cl atom chemisorbed onto the fcc site. The thin red and blue lines represent the integrated PDOS (right axis) for the two Cl atoms.

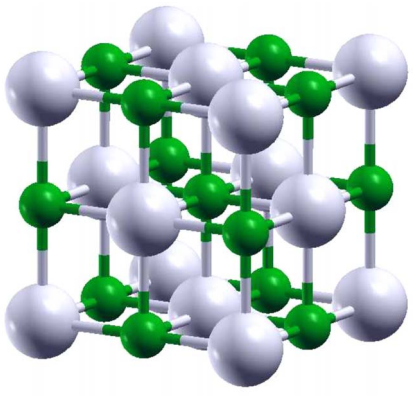

FIG. 5. (Color online) Crystal structure of silver chloride (AgCl).

site (Fig. 4, middle panel) the integration gives $\approx 7.2e$ for both Cl atoms, whereas for the chemisorbed Cl is $\approx 7.5e$ (Fig. 4, bottom panel), thus having a net additional charge of $0.5e$.

B. AgCl

In this section we report results for AgCl structure. AgCl is solid at standard temperature and pressure and the crystal structure is rocksalt, where each Ag atom has six Cl atoms as nearest neighbors, in an octahedral configuration and vice versa (Fig. 5). The study of AgCl is interesting since it may represent the limiting case of Cl adsorption on Ag structure in presence of very high Cl coverage.

The equilibrium lattice parameter and the bulk modulus have been calculated fitting total energy with the Murnaghan equation. Results are collected in Table II, where comparison with previous local-density approximation (LDA) study[35] and experimental results[35] is reported. Our calculated lattice parameter, a_0, is 5.61 Å and the bulk modulus B is 453 kbar. The binding energy of Cl atom in the AgCl structure, as obtained in this work, is −0.91 eV. This quantity is calculated with respect to a Ag atom in the bulk Ag and Cl_2 molecule in the gas phase, and it represents the energy gained per Cl atom to dissociate Cl_2 and to form AgCl from Ag bulk.

C. Cl on Ag(111)

In this section we present results for different Cl adsorption geometries on Ag(111) surface as a function of Cl coverage. We considered pure on-surface, subsurface, and substitutional adsorptions, as well as the mixed on-surface +subsurface and on-surface+substitutional adsorptions. Identified geometries and corresponding chemisorption energies per Cl atom are collected in Figs. 6–11 and Tables III–VI, where structural parameters are also reported.

When considering more than one Cl atom per (2×2) supercell, there are two different types of the same site, depending on the relative distance between Cl atoms. We refer to adjacent sites with label 1 nn (first nearest neighbors) and to the second-nearest-neighbor sites with label 2 nn. Unless specified otherwise, we always considered 2 nn sites since we expect a repulsive Cl–Cl interaction because adsorbed Cl displays a negative charge (about $0.5e$ at 1/4 ML, see Sec. III A).

TABLE II. Lattice constant and bulk modulus of AgCl as calculated in the present work compared to a previous LDA study and experiments.

	a_0 (Å)	B (kbar)
This work	5.61	453
LDA[a]	5.46	620
Expt.[a]	5.55	513

[a]Reference 35.

1. Relative stability of on-surface sites at low coverage

The results for the on-surface Cl adsorption are reported in Table III. The relative stability of high-symmetry on-surface sites at low coverage follows the order fcc≈hcp >bridge>top, and at 1/4 ML the corresponding chemisorption energies are −1.48, −1.47, −1.41, and −1.08 eV, respectively. However at this coverage, the bridge and top sites are not local minima, and the corresponding E_{chem} values have been obtained from constrained optimizations for comparison purposes. The difference between the chemisorption energies corresponding to hollow and bridge sites is quite small, below 0.1 eV, indicating a small diffusion barrier.

The hollow fcc and hcp adsorption sites remain the most stable also at coverage of 1/3 ML. In particular, our results at this coverage are in reasonable agreement with previous GGA studies.[14,16] We obtain a chemisorption energy of −1.52 eV, height of the Cl atom above the surface ($\Delta z^{\mathrm{on}}_{\mathrm{Cl-Ag}}$) of 1.98 Å, and Ag–Cl distance ($d^{\mathrm{on}}_{\mathrm{Cl-Ag}}$) of 2.64 Å. Doll and Harrison[14] predicted a chemisorption energy of −1.69 eV, $\Delta z^{\mathrm{on}}_{\mathrm{Cl-Ag}}$ of 2.01 Å, and $d^{\mathrm{on}}_{\mathrm{Cl-Ag}}$ of 2.62 Å, while de Leeuw *et al.*[16] predicted a chemisorption energy of −1.62 eV and $d^{\mathrm{on}}_{\mathrm{Cl-Ag}}$ of 2.66 Å.

2. On-surface adsorption at high coverage

At coverage of 1/2 ML, the most stable configuration we identified is the honeycomb structure shown in Fig. 6(a), where Cl atoms are adsorbed into fcc and hcp sites linked together by a Ag atom, thus forming the -Cl–Ag–Cl- hexagonal chains. The average chemisorption energy for this structure is −1.13 eV. For this coverage we identified several hexagonal on-surface configurations, and some of them are shown in Fig. 6. For instance, when Cl atoms are initially adsorbed on 1 nn fcc and hcp sites, the lateral repulsion displaces them toward the top sites, forming the hexagonal structure shown in Fig. 6(b), with an average chemisorption energy of −1.05 eV. This structure also forms when one Cl_2 molecule per (2×2) supercell is initially adsorbed over the 1 nn fcc-to-hcp sites with its axis parallel to the surface; the molecule then dissociates without barrier. Hexagonal structures shown in Figs. 6(c) and 6(d) are combinations of 2 nn fcc/top sites and 2 nn hcp/top sites, respectively. The average chemisorption energies are −1.06 and −1.04 eV, respec-

TABLE III. Structural parameters and chemisorption energies, E_{chem}, in eV/Cl atom for on-surface Cl configurations as a function of coverage, Θ_{on}. Other labels are defined in Sec. II. For pure Ag(111) $\Delta d_{12}=-0.7\%$.

Θ_{on} (ML)	Sites		E_{chem} (eV)	Δz^{on}_{Cl-Ag} (Å)	d^{on}_{Cl-Ag} (Å)	h_{Ag} (Å)	Δd_{12} (%)
1/16	fcc		−1.53	2.01	2.66	0.05	−0.9
1/9	fcc		−1.58	2.00	2.65	0.04	−1.6
1/4	fcc		−1.48	2.04	2.66	0.10	−1.6
	hcp		−1.47	2.04	2.66	0.06	−1.6
	Bridge[a]		−1.41				
	Top[a]		−1.08				
1/3	fcc		−1.52	1.98	2.64	0.00	−1.4
	hcp		−1.51	1.99	2.64	0.00	−1.2
1/2	fcc/hcp	Fig. 6(a)	−1.13	2.01	2.62	0.07	−1.4
	Off-fcc/off-hcp	Fig. 6(b)	−1.05	1.99	2.68	0.37	0.3
	fcc/top	Fig. 6(c)	−1.06	2.07	2.50	0.17	−0.9
	hcp/top	Fig. 6(d)	−1.04	2.07	2.52	0.20	−1.2
2/3	fcc/fcc	Fig. 7(a)	−0.70	1.96	2.61	0.00	−1.2
3/4	fcc/hcp/top	Fig. 7(b)	−0.75	2.07	2.54	0.10	−1.1

[a]Not a local minimum at this coverage.

tively. When Cl atoms are initially adsorbed on adjacent fcc sites the resulting geometry is a low-symmetry variant of the hexagonal structure shown in Fig. 6(c), whereas when Cl atoms are initially on adjacent hcp sites, the resulting structure is again Fig. 6(a). Similar results for Cl_2 dissociative adsorption have been reported by de Leeuw *et al.*[16]

By increasing Cl coverage to 2/3 ML, the most stable identified geometry is a honeycomb structure, shown in Fig. 7(a), where Cl atoms are adsorbed on 1 nn fcc sites with an average chemisorption energy of −0.70 eV. A hexagonal adsorbate configuration is preserved even at larger coverage of 3/4 ML; the most stable identified structure is shown in Fig. 7(b) with an average chemisorption energy of −0.75 eV. This structure is composed of Cl atoms adsorbed on 2 nn fcc and hcp sites forming the structure of Fig. 6(a), with an additional Cl atom adsorbed on the top site at the center of the hexagon, so as to minimize the repulsive lateral interaction. At high Cl coverage ($\Theta \geq 1/2$ ML) the average distance between Cl atoms and nearest-neighbor Ag surface atoms varies from 2.53 and 2.62 Å. We note that at $\Theta \geq 2/3$ ML, the pure on-surface Cl adsorption is thermodynamically less stable than formation of AgCl structure. This may indicate that at these high on-surface coverages Cl may prefer to go subsurface.

3. Subsurface adsorption

The results for the subsurface Cl adsorption are reported in Table IV. At low Cl coverage ($\Theta=1/4$ ML) pure subsurface adsorption is highly disfavored with respect to on-surface adsorption, and it results to be endothermic with a chemisorption energies of +0.76, +1.51, and +0.75 eV for the octa, tetra-1, and tetra-2 sites, respectively. This endothermicity can be attributed to large distortion of the surface: subsurface Cl atoms push up substantially top silver layer (Δd_{12} and in some cases also h^{surf}_{Ag} are very large) so as to

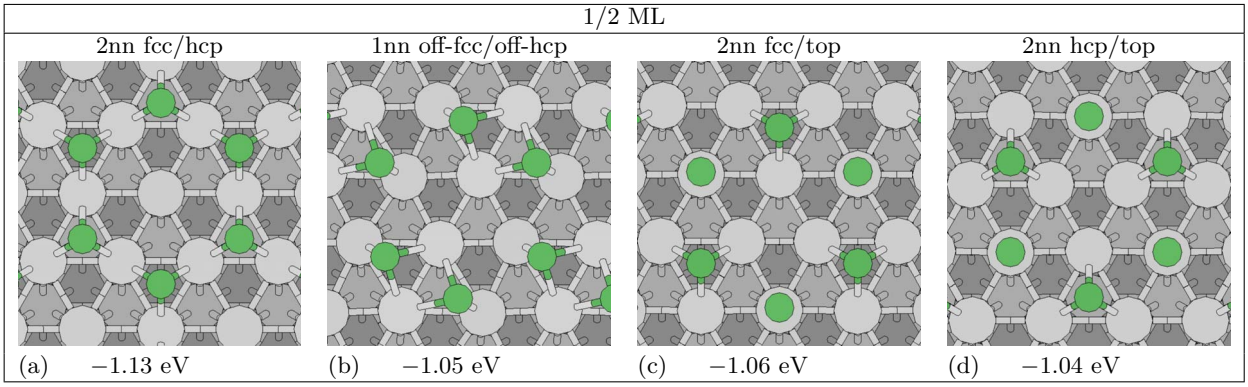

FIG. 6. (Color online) On-surface Cl adsorption configurations on Ag(111) at a total coverage of 1/2 ML, with corresponding average chemisorption energies, E_{chem}. All these structures display a honeycomb pattern. We identified also other structures, which are low-symmetry variants of these presented here.

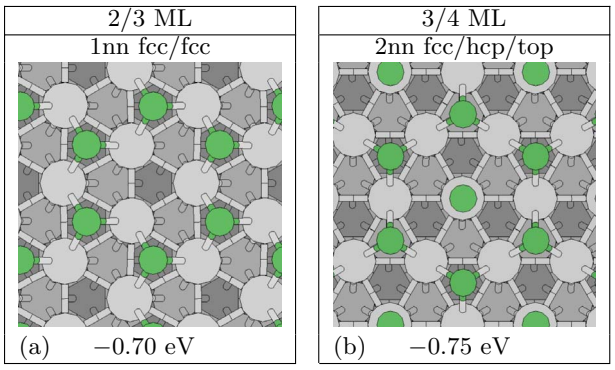

FIG. 7. (Color online) On-surface Cl configurations on Ag(111) at (a) 2/3 ML and (b) 3/4 ML, with corresponding average chemisorption energies, E_{chem}.

break the Ag–Ag bonds between the surface and subsurface layer.

By increasing the coverage to 1/3 ML, adsorption into tetra-1 sites remains endothermic (E_{chem} is 0.22 eV), while adsorption into octa and tetra-2 sites is athermic (E_{chem} is 0.02 and 0.01 eV, respectively). At this subsurface Cl coverage, Δd_{12} is still very high while there is no surface corrugation due to symmetry imposed by the supercell.

These numbers indicate that the subsurface adsorption becomes more stable with increasing coverage. For the sake of establishing a trend, we performed also few calculations at 1/2 and 3/4 ML coverages. At 1/2 ML we considered a geometry with one Cl atom in octa site and the other in the 2 nn tetra-2 site. We choose this configuration because these two sites are the most stable subsurface sites at lower coverage. At 3/4 ML we considered a configuration with the three Cl atoms located into octa, tetra-1, and tetra-2 subsurface sites. The resulting average chemisorption energies are −0.17 and −0.40 eV at 1/2 and 3/4 ML, respectively, in agreement with the trend anticipated above.

4. Mixed on-surface and subsurface adsorption

The results for the mixed on-surface+subsurface Cl adsorption are reported in Table V. The lowest coverage at which we investigated mixed on-surface+subsurface adsorption of Cl is 1/2 ML; this corresponds to one on-surface and one subsurface Cl atom per (2×2) supercell. At this coverage, we considered all six combinations with the on-surface Cl atom located in the most stable fcc and hcp sites and the subsurface Cl atom into 2 nn tetra-1, tetra-2, and octa sites.

During the geometry optimization, for some of these initial configurations the subsurface Cl atom is shifted on surface, whereas other structures result in a large restructuring of the surface, such as the formation of steps and Ag adatoms. The relaxation is therefore so substantial that optimized structures bear very little or no resemblance to initial Cl configurations. Nevertheless, to facilitate the discussion, in Table V we name all configurations according to their initial configurations, and in Figs. 8–10 initial (top row) and optimized (two bottom rows, side and top views) configurations are shown. On-surface Cl atoms are green, whereas Cl atoms below the uppermost Ag atoms are blue. Cl atoms in tetra-2 sites are located below Ag atoms marked with red cross (×).

Relaxation of fcc/octa and hcp/tetra-1 configurations results in pure on-surface Cl structures. In particular, the fcc/octa structure after geometry optimization coincides with the fcc/top structure shown in Fig. 6(c), whereas the optimized hcp/tetra-1 has an average chemisorption energy of −1.04 eV, and it is a low-symmetry variant of configuration shown in Fig. 6(d). For other structures the relaxation results in mixed on-surface+subsurface Cl configurations. The most stable is the hcp/tetra-2 structure [Fig. 8(f)] with an average chemisorption energy of −0.86 eV followed by the fcc/tetra-1 and hcp/octa [Figs. 8(b) and 8(d)] with E_{chem} of −0.61 eV. These three configurations display a steppedlike surface structure. The least stable mixed configuration is the fcc/tetra-2 [Fig. 8(c)], with E_{chem} of −0.42 eV. In this structure the Cl atom initially located in the tetra-2 site moved to a surface-substitutional position, pushing the Ag atom up above the surface level, thus effectively transforming it into an adatom.

At 2/3 ML we considered configurations with one Cl atom in fcc site and the other in octa, tetra-1, or tetra-2 subsurface sites. The three resulting configurations are shown in Figs. 8(g)–8(i), respectively. Due to smallness of $(\sqrt{3}\times\sqrt{3})R30°$ supercell, configurations fcc/tetra-1 and fcc/tetra-2 can only

TABLE IV. Structural parameters and chemisorption energies, E_{chem}, in eV/Cl atom for subsurface Cl configurations as a function of coverage, Θ_{sub}. Other labels are defined in Sec. II. For pure Ag(111) $\Delta d_{12}=-0.7\%$.

Θ_{sub} (ML)	Sites	E_{chem} (eV)	Δz^{sub}_{Cl-Ag} (Å)	d^{sub}_{Cl-Ag} (Å)	h_{Ag} (Å)	Δd_{12} (%)
1/4	Octa	0.76	−2.72	2.96	0.11	101.7
	Tetra-1	1.51	−1.45	2.57	1.53	57.0
	Tetra-2	0.75	−3.06	2.75	0.29	115.5
1/3	Octa	0.02	−2.86	3.02	0.00	106.5
	Tetra-1	0.22	−2.41	2.88	0.00	106.7
	Tetra-2	0.01	−2.99	2.75	0.18	110.6
1/2	Octa /tetra-2	−0.17	−2.91	2.91	0.18	108.8
3/4	Octa/tetra-1/tetra-2	−0.40	−2.28	2.63	0.07	80.7

TABLE V. Structural parameters and chemisorption energies, E_{chem}, in eV/Cl atom for mixed on-surface+subsurface Cl configurations. Label "Initial conf." refers to Cl configuration before the structural relaxation, whereas "Final conf." refers to figures where relaxed configurations are shown. Θ^f_{on} (Θ^f_{sub}) is the coverage of on-surface (subsurface) Cl atoms in the relaxed configuration. Other labels are defined in Sec. II. For highly reconstructed structures the evaluation of Δz_{Cl-Ag} and d_{Cl-Ag} becomes difficult, due to a substantial corrugation of the first two surface layers. For these structures, the two quantities are omitted, and moreover, the Θ^f_{on} and Θ^f_{sub} are evaluated with respect to the uppermost Ag atom.

Θ_{total} (ML)	Θ_{on} (ML)	Θ_{sub} (ML)	Initial conf.	Final conf.	E_{chem} (eV)	Θ^f_{on} (ML)	Θ^f_{sub} (ML)	Δz^{on}_{Cl-Ag} (Å)	Δz^{sub}_{Cl-Ag} (Å)	d^{on}_{Cl-Ag} (Å)	d^{sub}_{Cl-Ag} (Å)	h_{Ag} (Å)	Δd_{12} (%)
1/2	1/4	1/4	fcc/tetra-1	Fig. 8(b)	−0.61	1/4	1/4					2.30	42.8
			fcc/tetra-2	Fig. 8(c)	−0.42	0	1/2					3.25	31.3
			hcp/octa	Fig. 8(d)	−0.61	1/4	1/4					2.31	42.5
			hcp/tetra-2	Fig. 8(f)	−0.86							2.32	20.6
2/3	1/3	1/3	fcc/octa	Fig. 8(g)	−0.44	1/3	1/3	1.95	−2.43	2.63	2.98	0.00	94.2
			fcc/tetra-1	Fig. 8(h)	−0.47	1/3	1/3	2.09	−2.34	2.48	2.77	1.22	101.3
			fcc/tetra-2	Fig. 8(i)	−0.46	1/3	1/3	1.94	−2.98	2.64	3.64	0.54	113.2
3/4	1/2	1/4	fcc/hcp/octa	Fig. 9(a)	−0.87	0	3/4					2.85	28.2
			fcc/hcp/tetra-1	Fig. 9(b)	−0.87	1/4	1/2					2.47	23.8
			fcc/hcp/tetra-2	Fig. 9(c)	−0.87	0	3/4					2.86	28.0
			fcc/fcc/octa	Fig. 9(d)	−0.91	1/4	1/2					3.66	67.3
			fcc/fcc/tetra-1	Fig. 9(e)	−0.87	0	3/4					2.79	27.6
			fcc/fcc/tetra-2	Fig. 9(f)	−0.74	1/4	1/2					3.40	32.8
			hcp/hcp/ octa	Fig. 9(g)	−0.89	1/4	1/2					3.15	59.1
			hcp/hcp/tetra-1	Fig. 9(h)	−0.89	1/4	1/2					3.17	52.1
			hcp/hcp/tetra-2	Fig. 9(i)	−0.87	0	3/4					2.82	27.9
3/4	1/4	1/2	fcc/tetra-1/tetra-2	Fig. 10(a)	−0.44	1/4	1/2	2.03	−2.65	2.61	2.74	0.36	107.5
			hcp/octa/tetra-2	Fig. 10(b)	−0.46	1/4	1/2	2.05	−3.27	2.58	3.05	0.75	124.1

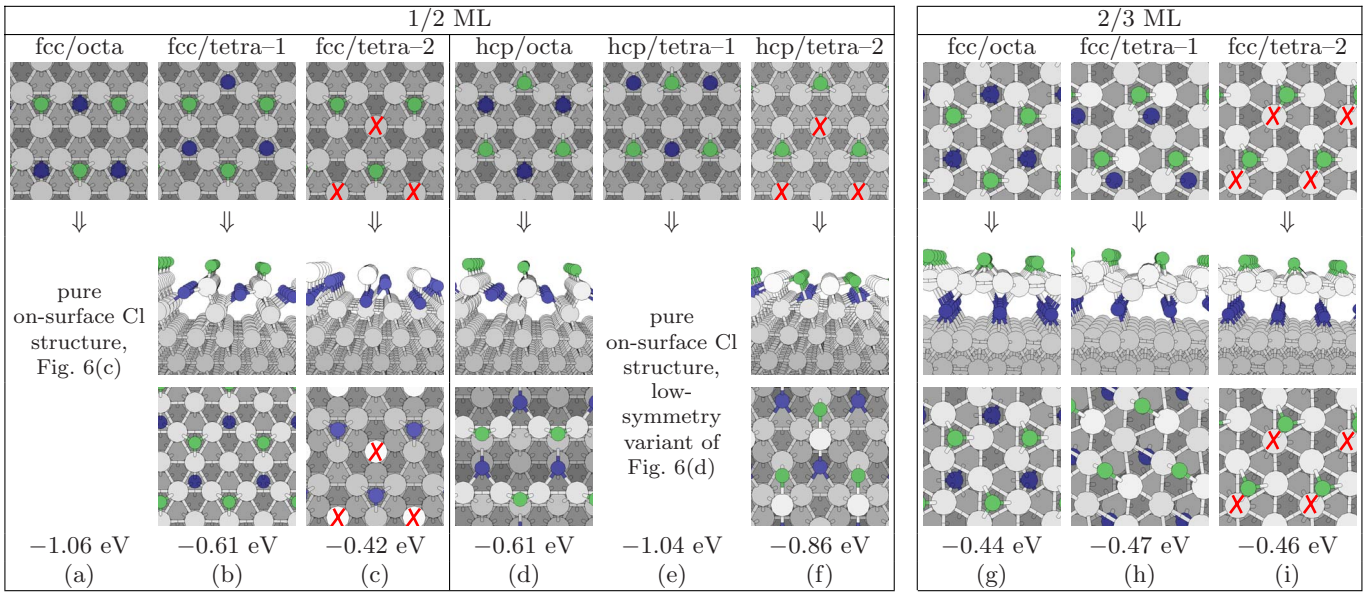

FIG. 8. (Color online) Mixed on-surface+subsurface Cl configurations on Ag(111) at a total coverage of [(a)–(f)] 1/2 ML and [(g)–(i)] 2/3 ML. Top row: initial configurations; two bottom rows: optimized configurations from side and top views. Corresponding average chemisorption energies are also reported. Cl atoms in tetra-2 sites are located below Ag atoms marked with red cross (×). Green balls: on-surface Cl atoms. Blue balls: Cl atoms below the uppermost Ag atoms. During the geometry optimization of the initial fcc/octa and hcp/tetra-1 structures shown in (a) and (e), top panel, the subsurface Cl migrates above the surface.

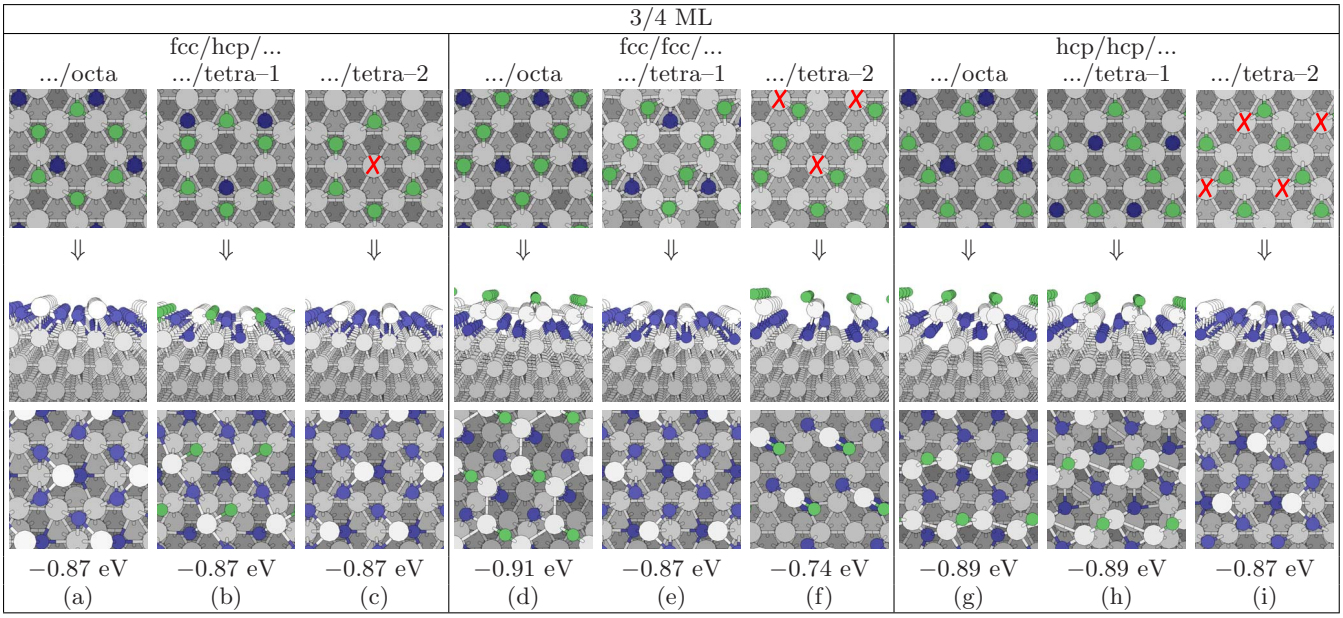

FIG. 9. (Color online) Mixed on-surface+subsurface Cl configurations on Ag(111) at a total coverage of 3/4 ML. Top row: initial configurations; two bottom rows: optimized configurations from side and top views. Corresponding average chemisorption energies are also reported. Cl atoms in tetra-2 sites are located below Ag atoms marked with red cross (×). Green balls: on-surface Cl atoms. Blue balls: Cl atoms below the uppermost Ag atoms.

be 1 nn [Figs. 8(h) and 8(i), top row]. In the final configurations of these three mixed on-surface+subsurface structures [Figs. 8(g)–8(i), two bottom rows] the top Ag layer is substantially shifted up due to subsurface Cl atoms. All the three resulting structures display similar average chemisorption energies, being −0.44, −0.47, and −0.46 eV for the fcc/octa, fcc/tetra-1, and fcc/tetra-2, respectively.

At coverage of 3/4 ML we considered initial configurations with 1/2 ML of on surface and 1/4 ML of subsurface Cl. This choice is suggested by the fact that at 1/2 ML coverage pure on-surface adsorption is the most stable. In particular, we investigated on-surface structures involving 2 nn fcc/hcp, 1 nn hcp/hcp, and 1 nn fcc/fcc sites combined with the octa, tetra-1, and tetra-2 subsurface sites. Since the number of possible combinations is too large, we explored nine configurations (shown in Fig. 9, top row), chosen such that the subsurface Cl is as far as possible from the two on-surface Cl atoms in the initial structure. Relaxation of these configurations involves large restructuring of surface, and optimized structures are shown in two bottom rows of Fig. 9. The average chemisorption energy is about −0.9 eV in the most stable structures. Therefore these configurations are more stable than the one shown in Fig. 7(b), which is the most stable identified purely on-surface configuration at 3/4 ML, indicating that at this coverage the mixed on-surface +subsurface adsorption is more stable than the pure on-surface one.

Interestingly, the optimized structures shown in Fig. 9 involve larger amount of subsurface Cl than anticipated above. In particular, structures shown in Figs. 9(a), 9(c), 9(e), and 9(i) contain all Cl atoms below the uppermost Ag atoms, whereas the other structures contain only 1/4 ML of on-surface Cl. For this reason we also investigated two structures with majority of subsurface Cl in the initial

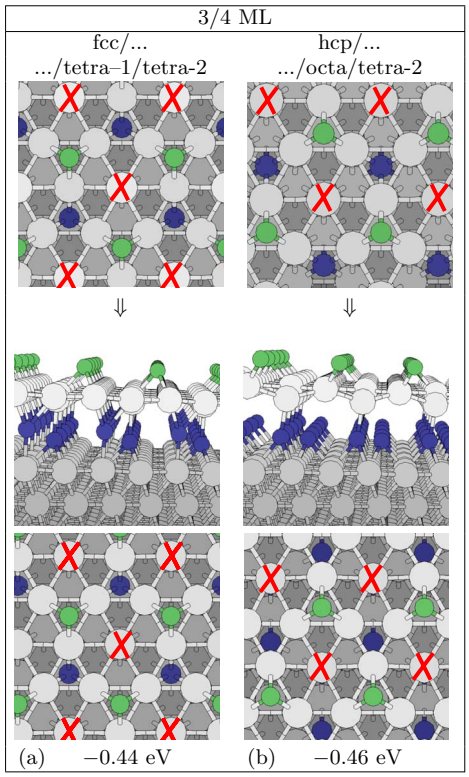

FIG. 10. (Color online) Mixed on-surface+subsurface Cl configurations on Ag(111) at a total coverage of 3/4 ML, with 1/2 ML of subsurface Cl. Top row: initial configurations; two bottom rows: optimized configurations from side and top views. Corresponding average chemisorption energies are also reported. Cl atoms in tetra-2 sites are located below Ag atoms marked with red cross (×). Green balls: on-surface Cl atoms. Blue balls: Cl atoms below uppermost Ag atoms.

TABLE VI. Structural parameters, substitutional chemisorption energy, E_{chem}^{subst}, and gross chemisorption energy on preformed vacancies, E_{chem}^{vac}, in eV/Cl atom on Ag(111) for pure substitutional and mixed on-surface+substitutional configurations. Θ_{tot} is the total Cl coverage; Θ_{on} (Θ_{subst}) is the coverage of on-surface (substitutional) Cl. "Vacancy layer" is the Ag layer containing the vacancies, which is either surface (first) or subsurface (second). Other labels are defined in Sec. II. For pure Ag(111) Δd_{12}=−0.7%.

Θ_{tot} (ML)	Θ_{on} (ML)	Θ_{subst} (ML)	Vacancy layer		E_{chem}^{subst} (eV)	E_{chem}^{vac} (eV)	Δz_{Cl-Ag}^{on} (Å)	Δz_{Cl-Ag}^{subst} (Å)	d_{Cl-Ag}^{on} (Å)	d_{Cl-Ag}^{subst} (Å)	h_{Ag} (Å)	Δd_{12} (%)
1/9	0	1/9	First	Fig. 11(a)	−1.00	−1.54		0.95		3.10	0.05	−1.36
			Second		0.17	−0.36		−2.50		2.94	0.12	1.0
1/4	0	1/4	First	Fig. 11(b)	−0.79	−1.38		1.06		3.13	0.00	−3.5
			Second		0.32	−0.27		−2.65		2.84	0.06	0.8
1/2	0	1/2	First	Fig. 11(c)	−1.00	−1.44		0.95		2.66	0.00	−3.6
	1/4	1/4	First	Fig. 11(d)	−1.09	−1.38	1.94	0.47	2.60	2.98	0.00	−1.4
3/4	1/2	1/4	First	Fig. 11(e)	−0.94	−1.14	1.94	−0.11	2.58	2.88	0.00	0.5

configuration, i.e., with 1/2 ML of subsurface and 1/4 ML of on-surface Cl atoms. In particular we considered fcc/tetra-1/tetra-2 and hcp/octa/tetra-2 structures because in these structures Cl atoms are as far apart as possible [Figs. 10(a) and 10(b), top row, respectively]. In the resulting optimized structures, the on-surface and subsurface coverages are unchanged [Figs. 10(a) and 10(b), two bottom rows, respectively], and the average chemisorption energies are −0.44 and −0.46 eV, respectively. Hence these two structures are less stable than those of Fig. 9. Moreover, the surface Ag layer is substantially less corrugated and completely detached from the subsurface Ag layer, being the two layers linked together only trough the subsurface Cl atoms.

5. Substitutional adsorption

Substitutional adsorption can be seen as adsorption into a vacancy, which is one of the possible surface defects and therefore a realistic adsorption site. Moreover substitutional adsorption can be a possible route for incorporation of Cl atoms below the surface. The results for the substitutional Cl adsorption are reported in Table VI.

We first calculated the surface vacancy formation energy (see Table VII). This slightly depends on the vacancy coverage, being 0.54 and 0.59 eV at 1/9 and 1/4 ML, respectively. We have also calculated the surface vacancy formation energy at 1/2 ML (0.44 eV). However, at this high coverage vacancies are merged into missing rows: the surface layer consists of alternative ridges and troughs.

Optimized geometries, corresponding to Cl substitutional adsorption into the surface layer at 1/9 and 1/4 ML, are shown in Figs. 11(a) and 11(b), respectively. Substitutional Cl atoms are represented with red balls. The substitutional chemisorption energies are −1.00 and −0.79 eV at 1/9 and 1/4 ML, respectively, whereas the gross chemisorption energies into a preformed on-surface vacancy are −1.54 and −1.38 eV, respectively. According to this result, at 1/9 ML the Cl binds similarly to vacancy and fcc site (E_{chem}=−1.58 eV), the difference being 0.04 eV in favor for the fcc site. This trend is in agreement with the result of de Leeuw *et al.*,[16] although our E_{chem} values are somewhat smaller.

TABLE VII. Vacancy formation energy, E_f, as a function of vacancy coverage, Θ_{vac}. h_{Ag}^{surf} is the difference in height between the highest and lowest surface Ag atoms. Δd_{12} is the relaxation of the surface layer. For pure Ag(111) Δd_{12}=−0.7%.

Θ_{vac} (ML)	E_f (eV/vac)	h_{Ag} (Å)	Δd_{12} (%)
1/9	0.54	0.03	−2.0
1/4	0.59	0.00	−3.7
1/2	0.44	0.00	−6.6

At 1/2 ML, the initial structure is composed of alternative Cl and Ag rows in the surface layer [see the inset of Fig. 11(c)]. However, during the structural optimization one Cl atom is pushed toward the bridge site and a honeycomb Cl configuration is formed. The average substitutional chemisorption energy is −1.00 eV, while the gross chemisorption energy on preformed vacancies (missing rows) would be −1.44 eV.

At 1/9 and 1/4 ML, we also investigated Cl substitutional adsorption into the first subsurface layer. The corresponding E_{chem}^{subst} are +0.17 and +0.32 eV, respectively, and are therefore substantially less stable than that for the surface layer. Based on these results, we may conclude that at low coverage, the substitutional adsorption is less stable than pure on-surface adsorption.

6. Mixed on-surface+substitutional adsorption

At 1/2 ML we also investigated a mixed on-surface +substitutional configuration, where 1/4 ML of Cl is substitutional and the other 1/4 ML is adsorbed on the 2 nn fcc sites [Fig. 11(d)]. The resulting average chemisorption energy is −1.09 eV, and it is very close to the average chemisorption energy of pure on-surface adsorption at this coverage (−1.13 eV). This result suggests that, by increasing Cl coverage, mixed on-surface+substitutional adsorption may become a competitive or even preferred mode of adsorption.

For this reason, we investigated at 3/4 ML a configuration shown in Fig. 11(e), which is derived from the most stable on-surface configuration at 1/2 ML [Fig. 6(a)], where the Ag atom in the center of the hexagon is substituted by Cl atom. This configuration has an average substitutional chemisorp-

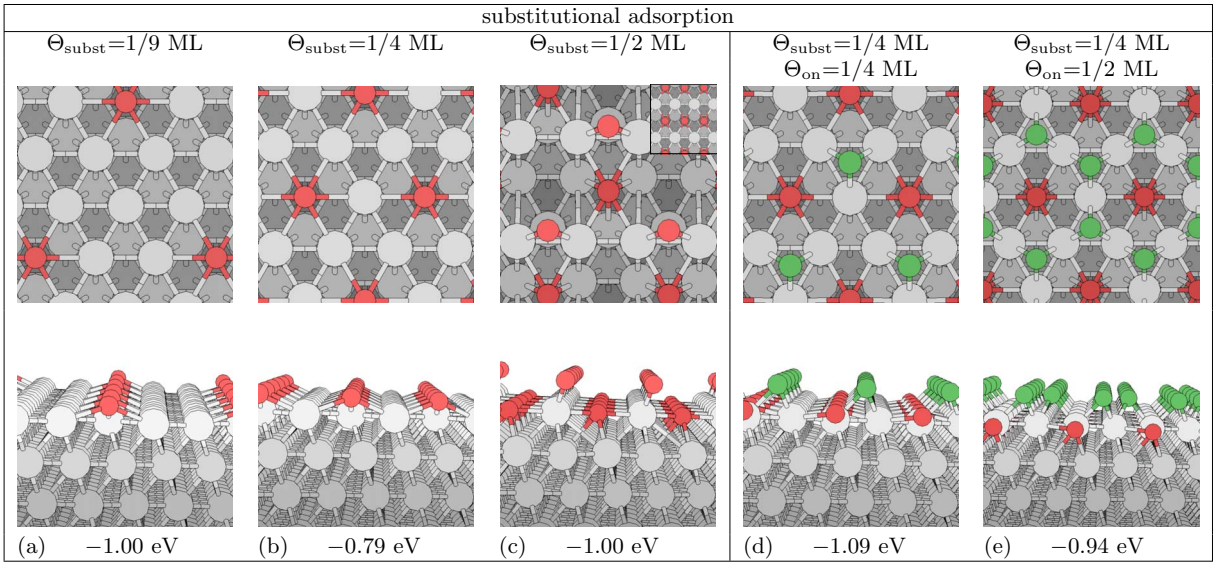

FIG. 11. (Color online) [(a)–(c)] Optimized substitutional Cl configurations on Ag(111) at coverages 1/9, 1/4, and 1/2 ML. The inset in (c) shows the corresponding initial structure. [(d) and (e)] Optimized mixed on-surface+substitutional Cl adsorption structures on Ag(111) at a total coverage of 1/2 and 3/4 ML. The average substitutional chemisorption energy, E_{chem}^{subst}, is also reported. Θ_{on} (Θ_{subst}) is the coverage of on-surface (substitutional) Cl. Red balls: substitutional Cl atoms. Green balls: on-surface Cl atoms.

tion energy of −0.94 eV. Therefore it is more stable than the pure on-surface adsorption (E_{chem}=−0.75 eV) and comparable with mixed on-surface+subsurface adsorption (E_{chem}=−0.91 eV).

IV. DISCUSSION

A. Trend of Cl chemisorption on Ag(111)

In Fig. 12 we show the trend of the average chemisorption energy of Cl on Ag(111), as a function of coverage and adsorption type, up to a 3/4 ML of coverage. Only the most stable structures for each adsorption type at a given coverage are considered. According to our results, the adsorption of Cl as a function of coverage can be classified into three regions.

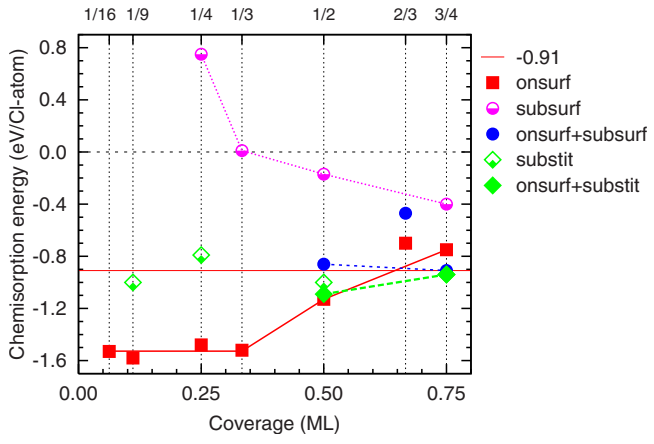

FIG. 12. (Color online) Average chemisorption energy of Cl adsorbed on Ag(111) as a function of coverage and adsorption type. The most stable on-surface, subsurface, mixed on-surface +subsurface, substitutional, and mixed on-surface+substitutional adsorption structures are considered for each coverage (designated as *onsurf*, *subsurf*, *onsurf+subsurf*, *substit*, and *onsurf+substit*, respectively). Red thin horizontal line at −0.91 eV corresponds to binding energy of Cl in AgCl bulk. Other lines are drawn to guide the eyes.

(i) $\Theta \leq 1/3$ ML: the on-surface adsorption is the most stable adsorption mode, and it is approximately independent on the coverage.

(ii) $1/3 \leq \Theta \leq 1/2$ ML: the on-surface adsorption mode remains the most stable, but the magnitude of chemisorption energy decrease with increasing coverage, and at about 1/2 ML the mixed on-surface+substitutional adsorption mode becomes competitive.

(iii) $\Theta > 1/2$ ML: at larger coverages the mixed adsorption modes become more stable than pure on-surface adsorption. This is completely consistent with the experimentally determined saturation coverage for the Cl overlayers, which is about 0.5–0.6 ML,[9,10] and with the observation that upon larger exposure of chlorine, the AgCl forms.[11]

1. Incommensurate Cl overlayers

As for the on-surface adsorption, various overlayer structures have been reported experimentally, depending on the conditions. At coverages around 1/3 ML, diffuse[8] and sharp[12] $(\sqrt{3}\times\sqrt{3})R30°$ as well as the (13×13) (Ref. 12) overlayer structures have been observed. Overlayers with various periodicities have been reported also at coverages around 1/2 ML, such as (10×10) (Refs. 8 and 12) and (17×17).[10] A common feature of these superstructure overlayers is that within the superstructure the Cl overlayer is locally incommensurate with Ag(111) surface.[10,12] This implies that Cl atoms bind not only to the most stable fcc/hcp sites but also to less stable bridge, top, and other intermediate positions.[10,12]

Although the structures considered in our calculations are commensurate due to the periodic nature of the computational method (see Ref. 36), our results give some useful

insight into why incommensurate overlayers appear. First, we note that at low coverage the chemisorption energy difference between various sites is small (see Table III), and moreover various calculated overlayer structures with Cl adsorbed on nonoptimal sites are comparable in energy to the most stable configuration (e.g., see Fig. 6). Therefore we deduce that the formation of various observed overlayer superstructures is driven by the lateral electrostatic repulsion between negatively charged Cl adatoms, which rearrange so as to maximally avoid each other, and therefore pushing some fraction of them toward otherwise less stable (bridge and top) sites. We further note that a large number of relaxed Cl configurations—both on surface and mixed—display a honeycomb pattern with either void or centered hexagons (e.g., see Figs. 6–9). Those rare configurations that do not are substantially less stable. This provides yet another evidence that Cl atoms arrange themselves so as to maximally avoid each other.

2. Subsurface and substitutional adsorption

Pure subsurface adsorption is the least stable adsorption mode at all considered coverages. However, its stability increases with increasing Cl coverage, hence displaying an opposite trend compared to on-surface adsorption mode. As for the stability of substitutional adsorption (including the mixed on-surface+substitutional mode at high coverages), it displays a constant trend with respect to coverage, with a chemisorption energy oscillating around −0.95 eV by about ±0.15 eV.

According to our results, large amount of adsorbed Cl ($\Theta \geq 1/2$ ML) induces large surface restructuring, which is in agreement with experimental findings.[2,13] In particular we note that relaxations of initial mixed on-surface+subsurface configurations produce three types of adsorption structures: (1) Cl atoms adsorbed solely on surface [Figs. 8(a) and 8(e)]; (2) structures involving large restructuring or corrugation of the surface [Figs. 8(b)–8(d) and 8(f), and Fig. 9]; and (3) on-surface+subsurface Cl configurations with less corrugated surface than type-2 structures [Figs. 8(g)–8(i), and Fig. 10].

In general, corrugated type-2 structures are more stable than "flat" type 3. This may be attributed to the following: type-3 structures involve in substantial relaxation of the surface layer, Δd_{12}, hence all direct surface-to-subsurface metal bonds are broken [see Figs. 8(g)–8(i) , and Fig. 10]. At variance, not all surface-to-subsurface metal bonds are broken when large corrugation of the surface layer occurs, and correspondingly Δd_{12} relaxation is substantially smaller. Less stable type-3 structures basically arise due to artifacts of the computational model that are related to finite-size effects. An example can be seen in Fig. 12: the two points at 2/3 ML have less exothermic E_{chem} than might be expected from interpolation between the two surrounding coverages; these points are obtained with a smaller $(\sqrt{3}\times\sqrt{3})R30°$ supercell, which does not allow for a corrugation of the on-surface +subsurface configuration.

Although we have studied a relatively large set of structures, there may be other, more stable, nonidentified structures. This is particularly true for the mixed on-surface +subsurface configurations, which display very complicated structures, with large corrugation of the metal layers. In these cases the most stable corrugation patterns may require larger supercells than the currently used (2×2). Nonetheless we believe we have captured the main trend.

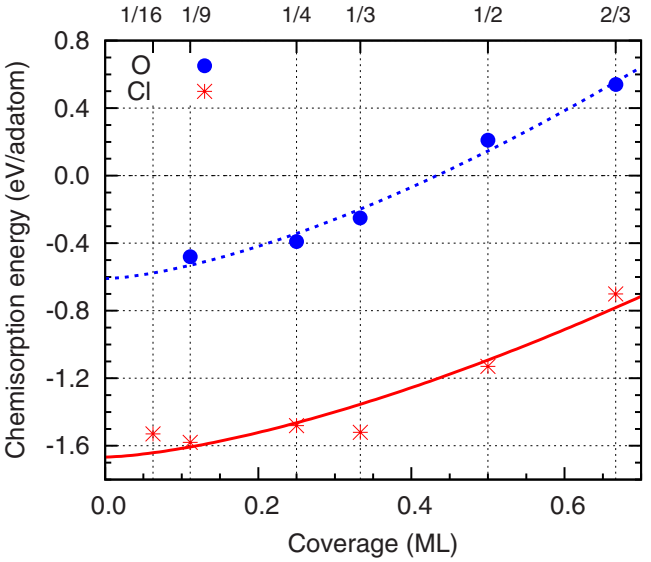

FIG. 13. (Color online) Comparison of chemisorption energy of Cl and O adsorbed on Ag(111) as a function of coverage. The data for O/Ag(111) adsorption are taken from Ref. 37. The two curves display the $\Theta^{3/2}$ dependence [$E=a+b\Theta^{3/2}$, i.e., fit to Eq. (7)].

B. Comparison between Cl and O chemisorptions

The adsorption of Cl on Ag bears some resemblance to that of oxygen: for both adsorbates the on-surface hollow sites are the most stable at low coverage, and the adsorption into subsurface sites becomes competitive at some critical coverage, mainly due to increasing lateral repulsive electrostatic interactions between adsorbates with increasing coverage. For O on Ag(111) the critical coverage is around 1/4 ML,[19] whereas on Ag(100) it is somewhat larger, about 1/2 ML.[18,23] For Cl on Ag(111) we have shown that the critical coverage is between 1/2 and 3/4 ML, hence larger than for O. This is not surprising because (i) the stability of subsurface adsorption was shown to depend strongly on the lattice deformation cost,[22] and (ii) the Cl atom is bigger than O, therefore requiring larger lattice deformation for the inclusion into subsurface sites. Moreover, (iii) the electrostatic repulsion between O adatoms should be larger than between Cl adatoms. The latter can be deduced from the dependence of chemisorption energy on coverage.

Both O and Cl are negatively charged on Ag(111); according to Löwdin population analysis the net additional electronic charges are $0.9e$ and $0.5e$, respectively. At not too high coverage, the main source of lateral adsorbate-adsorbate repulsion is therefore due to adsorbate induced dipoles (i.e., dipole-dipole interaction). This interaction scales as R^{-3}; hence for rather uniform adsorbate distributions this should scale with coverage as $\Theta^{3/2}$. As a rough estimate of lateral repulsion energy we write

$$E_{\text{rep}} \propto \frac{\mu^2}{R(\Theta)^3}\Sigma_{\text{lattice}} \approx \mu^2\Theta^{3/2}\Sigma_{\text{lattice}}, \tag{7}$$

where μ is the adsorbate induced dipole moment, $R(\Theta)$ is the adsorbate-adsorbate nearest-neighbor distance (and hence depends on the coverage Θ), and Σ_{lattice} is a lattice sum due to summation of an infinite two-dimensional array of dipoles and depends solely on the type of the adsorbate lattice.

In Fig. 13, we fit the chemisorption energy of Cl and O on Ag(111) as a function of coverage (up to $\Theta=2/3$ ML) by the relation $E=a+b\Theta^{3/2}$ [i.e., Eq. (7) with neglected variations of Σ_{lattice}]. The fit reveals that the lateral repulsion for O adatoms is larger than that for Cl adatoms since the corresponding b is 2.14 and 1.63, respectively. According to Eq. (7) the ratio between the slopes from O and Cl curves should be proportional to μ_O^2/μ_{Cl}^2. Roughly estimating the induced dipole as $\mu \propto q_{\text{Löwdin}}\Delta z$, where $q_{\text{Löwdin}}$ is the adatom net additional Löwdin charge and Δz its height above the surface, we obtain for the ratio $\mu_O^2/\mu_{Cl}^2=1.27$ being close to the ratio of the curve's slopes displayed in Fig. 13, $b_O/b_{Cl}=1.31$.

Despite the fact that the adsorbate-adsorbate repulsion is larger for O than for Cl, the formation of various adsorbate superstructures—discussed in Sec. IV A—which is driven by lateral electrostatic repulsion, is more characteristic of Cl adsorption. The reason is that the potential-energy surface for Cl adsorption is substantially flatter than that for O adsorption. In particular, for Cl at 1/4 ML the bridge and top sites are merely 0.1 and 0.4 eV less stable than the stablest fcc site (see Table III), whereas, according to our calculations, these differences are substantially larger for O, being 0.3 and 1.5 eV at 1/4 ML, respectively. Therefore, in the case of O adsorption the site preference wins over the lateral repulsion.

C. Does Cl go subsurface?

The E_{chem} trend of Cl adsorption discussed above indicates that at high Cl coverage the energetically most favored structures involve Cl in subsurface and/or substitutional sites. To make a link between the E_{chem} and the effect of temperature and chlorine partial pressure on various adsorption structures containing different amounts of Cl, we considered the surface free energy, γ, as a function of chlorine chemical potential, μ_{Cl}. The surface free energy is defined as

$$\gamma = \frac{G-[N_{Ag}\mu_{Ag}+N_{Cl}\mu_{Cl}]}{A}, \tag{8}$$

where A is the area of the surface unit cell, N_{Ag} and N_{Cl} are numbers of Ag and Cl atoms per supercell, respectively, and G is the Gibbs free energy. We define the adsorption free energy per unit area as the surface free-energy difference between chlorinated and clean surface, $\gamma_{\text{ads}} = \gamma_{Cl/Ag(111)} - \gamma_{Ag(111)}$, which is equal to

$$\gamma_{\text{ads}} = \frac{\Delta G-[\Delta N_{Ag}\mu_{Ag}+N_{Cl}\mu_{Cl}]}{A}, \tag{9}$$

where $\Delta G=G_{Cl/Ag(111)}-G_{Ag(111)}$. ΔG is approximated by the difference between the energies of the adsorption system, $E_{Cl/Ag(111)}$, and clean surface, $E_{Ag(111)}$. ΔN_{Ag} is the difference between the number of Ag atoms in the chlorinated and clean surface and is different from zero only for substitutional adsorption. We choose the reference state of μ_{Ag} to be the total energy of Ag atom in the bulk, $\mu_{Ag}=E_{Ag(bulk)}$, and the zero reference state of μ_{Cl} to be the total energy of Cl in isolated chlorine molecule, $\mu_{Cl}=\frac{1}{2}E_{Cl_2}=0$. With this choice, the average chemisorption energy of chlorine, E_{chem} [defined by Eq. (2)], and the adsorption free energy are related by

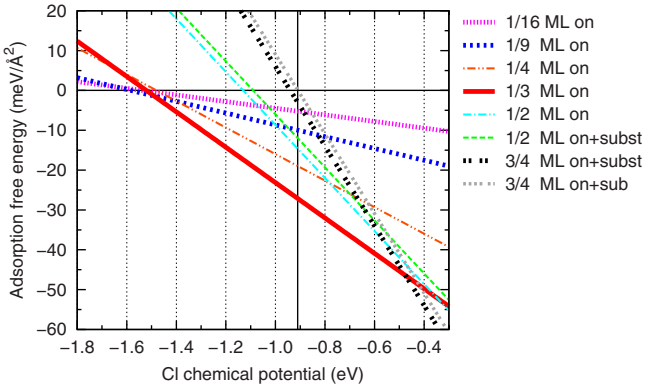

FIG. 14. (Color online) Adsorption free energy, γ_{ads}, for several low energy Cl/Ag(111) structures as a function of Cl chemical potential, μ_{Cl}. Horizontal black line at $\gamma_{\text{ads}}=0.0$ meV/Å^2 corresponds to clean Ag(111) surface. Vertical black line at $\mu_{Cl}=-0.91$ eV corresponds to bulk AgCl, whereas $\mu_{Cl}=0.0$ eV corresponds to isolated chlorine molecule. Labels *on*, *sub*, and *subst* stand for on-surface, subsurface, and substitutional chlorine, respectively.

$$\gamma_{\text{ads}} = \frac{N_{Cl}(E_{\text{chem}}-\mu_{Cl})}{A}. \tag{10}$$

For more details about such treatment, see Refs. 20 and 38. In Fig. 14 we display the adsorption free energy as a function of chlorine chemical potential for the identified most stable structures with on-surface (on), on-surface+subsurface (on+sub), and on-surface+substitutional (on+subst) Cl adsorptions at various coverages. The black horizontal line at $\gamma_{\text{ads}}=0$ meV/Å^2 and black vertical line at $\mu_{Cl}=-0.91$ eV correspond to clean Ag(111) surface and bulk AgCl, respectively. In this figure, we can distinguish four distinctive regimes. (i) At Cl chemical potentials below −1.6 eV, the clean Ag(111) surface is the most stable. (ii) Around $\mu_{Cl}\approx-1.5$ eV there is a narrow region where the low coverage on-surface structures at 1/16 and 1/9 ML are almost degenerate and the most stable (blue and purple lines). Also the on-surface 1/4 ML structure displays similar stability in this region (thin dotted-dashed orange line): the differences between them are not significant and within our estimated computational accuracy. (iii) Over a very broad range of μ_{Cl}, from −1.5 up to −0.5 eV, the most stable structure is the on-surface $(\sqrt{3}\times\sqrt{3})R30°$ at $\Theta=1/3$ ML (red thick line). This is in nice agreement with experimental observations, where the 1/3 ML coverage dominates [i.e., $(\sqrt{3}\times\sqrt{3})R30°$-Cl and other superstructures such as (13×13)].[8,12] (iv) For $\mu_{Cl}>-0.5$ eV, mixed on-surface +substitutional and on-surface+subsurface structures at 3/4 ML are the most stable and are almost degenerate (black and

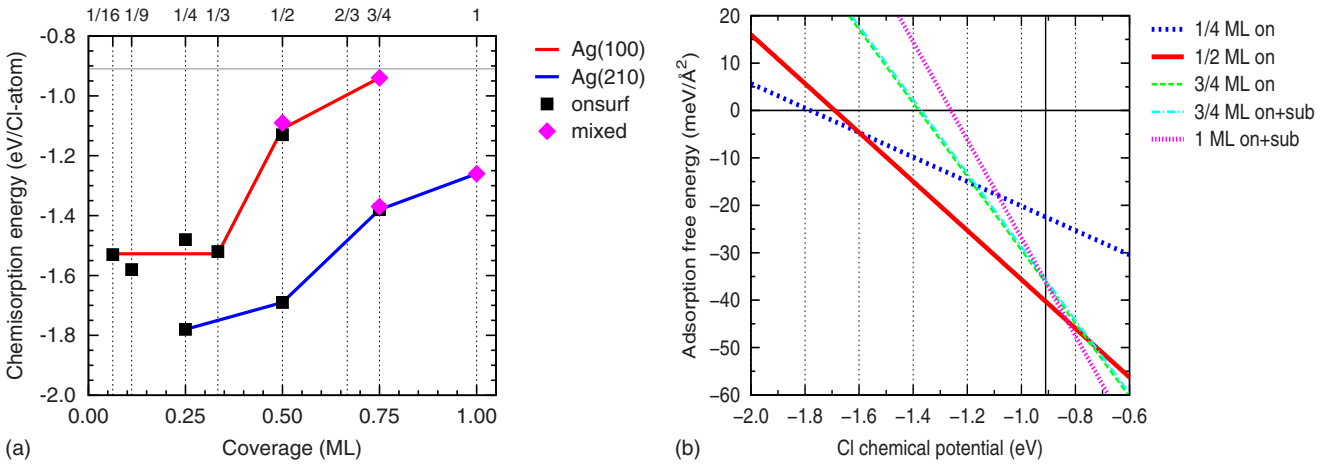

FIG. 15. (Color online) (a) Comparison between chemisorption energy of Cl on Ag(111) [red line] and Ag(210) [blue line] as a function of coverage. Only the most stable configurations at each coverage are plotted. Black rectangles and purple diamonds designate pure on-surface and mixed configurations, respectively. The horizontal line at −0.91 eV corresponds to binding energy of Cl in AgCl bulk. (b) Adsorption free energy, γ_{ads}, as a function of Cl chemical potential, μ_{Cl}, for several low energy Cl/Ag(210) structures. Horizontal black line at $\gamma_{ads}=0.0$ meV/Å^2 corresponds to clean Ag(210) surface, whereas vertical black line at $\mu_{Cl}=-0.91$ eV corresponds to bulk AgCl. Labels on and on+sub stand for on-surface and mixed on surface+subsurface, respectively.

gray dashed lines). Notice, however, that the bulk AgCl is thermodynamically more stable than these latter mixed on-surface+subsurface and on-surface+substitutional structures. Therefore the formation of these mixed adsorption structures can only be kinetically favored.

D. Role of surface defects

It has been demonstrated recently that the incorporation of oxygen below the surface strongly depends on lattice deformation properties.[22] For example, even if the stability of the corresponding oxides is comparable on silver and ruthenium, the critical coverage for incorporation below the surface is smaller on silver due to smaller lattice deformation cost. Furthermore, it has been shown that the subsurface incorporation is assisted by the presence of surface defects, such as steps,[24,25,39,40] where crystal structure is less rigid. In particular, the amount of steps, as well as very limited terrace width, is essential for oxide formation under UHV conditions.[41] For this reason we also investigated whether the presence of low coordinated steps facilitates the adsorption of Cl below the surface. We deliberately chose a very open surface, Ag(210), which consists of one-atom row wide (110) and (100) nanofacets.

According to our results, Cl binds more strongly to the step edge of Ag(210) than to perfect Ag(111) facet,[42] in agreement with results of de Leeuw *et al.*,[16] who studied Cl adsorption on stepped Ag(111) surface. The difference in E_{chem} between (111) and (210) is about a quarter of eV at low coverage ($\leq 1/4$ ML) and increases to about half of eV at high coverage. Nevertheless, our results indicate that low coordinated surface defects do not facilitate subsurface adsorption of Cl at low coverage. Instead, the tendency of Cl to stay on the surface at low coverage is even stronger that on perfect (111) facet. The more open (210) surface is easily deformed, thus allowing subsurface Cl to escape up onto the surface. Indeed all calculations at coverages $\leq 1/2$ ML, with subsurface Cl, resulted in pure on-surface adsorption structures, while on Ag(111) the mixed-type adsorption becomes competitive to pure on-surface adsorption at around 1/2 ML. On Ag(210) the mixed on-surface+subsurface adsorption becomes comparable to pure on-surface adsorption at coverages around 3/4 ML, whereas at around 1 ML the lateral electrostatic repulsion is so large that optimized configurations consist of some amount of Cl located below the surface even when the initial Cl configurations are purely on surface.

The stronger binding of Cl into Ag(210) compared to Ag(111) has an interesting thermodynamic consequence: on Ag(111) the mixed on-surface+subsurface adsorption becomes thermodynamically the most stable adsorption phase at Cl chemical potential around −0.5 eV (see Fig. 14), far beyond the −0.91 eV value where the AgCl becomes thermodynamically favored. On the other hand, on Ag(210) the mixed on-surface+subsurface adsorption becomes the most stable adsorption phase at Cl chemical potential around −0.85 eV [see Fig. 15(b)], thus very close to the onset of AgCl formation.

V. CONCLUSIONS

In this paper, we have used DFT-GGA calculations to address the adsorption of Cl on Ag(111) and its possibility to adsorb below the surface. As for the chemisorption energy of Cl, the adsorption as a function of coverage can be classified into three regions: (i) at coverages up to 1/3 ML the on-surface adsorption is far the most stable adsorption mode, with chemisorption energy being roughly independent of the coverage; (ii) for coverages between 1/3 and 1/2 ML, the on-surface adsorption remains the most stable adsorption mode, but the magnitude of chemisorption energy decreases with increasing coverage; and (iii) at coverages around 1/2 ML the mixed adsorption modes (on surface+subsurface and/or substitutional) become competitive and even preferred at higher coverages.

The analysis of adsorption free energy as a function of chlorine chemical potential reveals that the on-surface $(\sqrt{3}\times\sqrt{3})R30°$ adsorption phase is thermodynamically the most stable over a very broad range of Cl chemical potential. Only at a very low Cl chemical potential, around −1.5 eV, the low coverage configurations [i.e., (3×3) and (4×4)] are the most stable structures. Our results further indicate that the formation of various observed Cl overlayer superstructures at $\Theta\in[\frac{1}{3},\frac{1}{2}]$ ML, such as (13×13) and (10×10), is driven by the lateral electrostatic repulsion between negatively charged Cl adatoms. In particular, due to a small site preference, they are able to arrange so as to maximally avoid each other. As for the mixed adsorption modes at 3/4 ML coverage, they become thermodynamically the most stable phases at Cl chemical potential above −0.5 eV. The bulk AgCl is however thermodynamically more stable and would form at $\mu_{Cl}=-0.91$ eV. Hence the formation of mixed adsorption phases, if they would ever occur, cannot be due to thermodynamic equilibrium but can only result from kinetic effects.

Moreover, we found that the subsurface Cl adsorption at low coverage is not stabilized by the presence of open surface steps, such as in Ag(210). At high Cl coverage, the mixed on-surface+subsurface adsorption on Ag(210) becomes thermodynamically the most stable phase at Cl chemical potential of about −0.85 eV, thus close to the onset of bulk AgCl formation. Our calculations therefore strongly indicate that the presence of subsurface Cl at low coverage is improbable, and the assumption that Cl acts as a promoter in the ethylene epoxidation reaction when it is adsorbed subsurface should be likely revised.

[1] R. A. van Santen, in *Handbook of Heterogeneous Catalysis* (Wiley, Weinheim, Germany, 1997), Vol. 5, Chap. 4.6.1, pp. 2244–2252.
[2] J. G. Serafin, A. C. Liu, and S. R. Seyedmonir, J. Mol. Catal. A: Chem. **131**, 157 (1998).
[3] J. T. Jankowiak and M. A. Barteau, J. Catal. **236**, 379 (2005).
[4] S. Linic and M. A. Barteau, J. Am. Chem. Soc. **126**, 8086 (2004).
[5] M. Bowker and K. C. Waugh, Surf. Sci. **134**, 639 (1983).
[6] H. Piao, K. Adib, and M. A. Barteau, Surf. Sci. **557**, 13 (2004).
[7] M. Atkins, J. Couves, M. Hague, B. H. Sakakini, and K. Waugh, J. Catal. **235**, 103 (2005).
[8] P. J. Goddard and R. M. Lambert, Surf. Sci. **67**, 180 (1977).
[9] J. H. Schott and H. S. White, J. Phys. Chem. **98**, 291 (1994).
[10] B. V. Andryushechkin, K. N. Eltsov, V. M. Shevlyuga, and V. Y. Yurov, Surf. Sci. **407**, L633 (1998).
[11] V. Andryushechkin, K. N. Eltsov, and V. M. Shevlyuga, Surf. Sci. **433-435**, 109 (1999).
[12] A. G. Shard and V. R. Dhanak, J. Phys. Chem. B **104**, 2743 (2000).
[13] E. R. Frank and R. J. Hamers, J. Catal. **172**, 406 (1997).
[14] K. Doll and N. M. Harrison, Phys. Rev. B **63**, 165410 (2001).
[15] Y. Wang, Q. Sun, K. Fan, and J. Deng, Chem. Phys. Lett. **334**, 411 (2001).
[16] N. H. de Leeuw, C. J. Nelson, C. R. A. Catlow, P. Sautet, and W. Dong, Phys. Rev. B **69**, 045419 (2004).
[17] A. Migani and F. Illas, J. Phys. Chem. B **110**, 11894 (2006).
[18] A. Kokalj, A. Dal Corso, S. de Gironcoli, and S. Baroni, J. Phys. Chem. B **110**, 367 (2006).
[19] W.-X. Li, C. Stampfl, and M. Scheffler, Phys. Rev. B **67**, 045408 (2003).
[20] W.-X. Li, C. Stampfl, and M. Scheffler, Phys. Rev. B **68**, 165412 (2003).
[21] W.-X. Li, C. Stampfl, and M. Scheffler, Phys. Rev. Lett. **90**, 256102 (2003).
[22] M. Todorova, W. X. Li, M. V. Ganduglia-Pirovano, C. Stampfl, K. Reuter, and M. Scheffler, Phys. Rev. Lett. **89**, 096103 (2002).
[23] M. Gajdoš, A. Eichler, and J. Hafner, Surf. Sci. **531**, 272 (2003).
[24] L. Vattuone, L. Savio, and M. Rocca, Phys. Rev. Lett. **90**, 228302 (2003).
[25] A. Kokalj, N. Bonini, A. Dal Corso, S. de Gironcoli, and S. Baroni, Surf. Sci. **566-568**, 1107 (2004).
[26] J. P. Perdew, K. Burke, and M. Ernzerhof, Phys. Rev. Lett. **77**, 3865 (1996).
[27] D. Vanderbilt, Phys. Rev. B **41**, 7892 (1990).
[28] H. J. Monkhorst and J. D. Pack, Phys. Rev. B **13**, 5188 (1976).
[29] M. Methfessel and A. T. Paxton, Phys. Rev. B **40**, 3616 (1989).
[30] S. Baroni, A. Dal Corso, S. de Gironcoli, and P. Giannozzi, PWSCF and PHONON: plane-wave pseudopotential codes, 2005, http://www.pwscf.org/
[31] S. Baroni *et al.*, QUANTUM ESPRESSO: open-source package for research in electronic structure, simulation, and optimization, 2005, http://www.quantum-espresso.org/
[32] A. Kokalj, Comput. Mater. Sci. **28**, 155 (2003); code available from http://www.xcrysden.org/
[33] G. Henkelman and H. Jonsson, J. Chem. Phys. **113**, 9978 (2000).
[34] G. Henkelman, B. P. Uberuaga, and H. Jonsson, J. Chem. Phys. **113**, 9901 (2000).
[35] F. Kirchhoff, J. M. Holender, and M. J. Gillan, Phys. Rev. B **49**, 17420 (1994).
[36] In principle it would be possible to treat the experimentally determined incommensurate Cl overlayers, but corresponding calculations would involve rather large supercells, such as (17×17) and (13×13), and would require an overlarge computational resources.
[37] W.-X. Li, C. Stampfl, and M. Scheffler, Phys. Rev. B **65**, 075407 (2002).
[38] K. Reuter and M. Scheffler, Phys. Rev. B **65**, 035406 (2001).
[39] L. Savio, A. Gerbi, L. Vattuone, A. Baraldi, G. Comelli, and M. Rocca, J. Phys. Chem. B **110**, 942 (2006).
[40] N. Bonini, A. Dal Corso, A. Kokalj, S. de Gironcoli, and S. Baroni, Surf. Sci. **587**, 50 (2005).
[41] L. Savio, C. Giallombardo, L. Vattuone, A. Kokalj, and M. Rocca, J. Phys.: Condens. Matter **20**, 224006 (2008).
[42] P. Gava, A. Kokalj, S. de Gironcoli, and S. Baroni (unpublished).